

## Slope streak formation and dust deposition rates on Mars

Oded Aharonson, Norbert Schorghofer, and Marguerite F. Gerstell

Division of Geological and Planetary Sciences, California Institute of Technology, Pasadena, California, USA

Received 23 May 2003; revised 21 August 2003; accepted 24 October 2003; published 23 December 2003.

[1] The Mars Orbiter Camera (MOC) has imaged, sometimes repeatedly, mass movements known as slope streaks, which are abundant in the dust-covered regions on Mars. They are among the few known examples of contemporary surface changes. A survey of 173 collocated image pairs indicates that these features are currently forming at a high rate of  $\sim 7\%$  per existing streak, per Martian year. Either there is a complete turnover within a few decades or the streak population is currently increasing rapidly. Large spatial, as well as possible temporal, variations in the formation rate are obtained from these data. Streaks do not appear to fade over time periods comparable to their inverse formation rate of  $\sim 28$  years, as seen by analysis of Viking Orbiter images containing streaks that are still visible in MOC images. Gradual or stochastic variations in dust deposition may be needed to explain observations of changes in the formation rate, and its current imbalance with the fading rate. *INDEX TERMS*: 6225 Planetology: Solar System Objects: Mars; 5464 Planetology: Solid Surface Planets: Remote sensing; 5470 Planetology: Solid Surface Planets: Surface materials and properties; *KEYWORDS*: Mars, slope streaks, dust deposition, surface change

**Citation:** Aharonson, O., N. Schorghofer, and M. F. Gerstell, Slope streak formation and dust deposition rates on Mars, *J. Geophys. Res.*, 108(E12), 5138, doi:10.1029/2003JE002123, 2003.

### 1. Introduction

[2] Slope streaks are features forming on the surface of present-day Mars. They were first discovered in Viking Orbiter images [Morris, 1982; Ferguson and Lucchitta, 1984], and recently Mars Orbiter Camera (MOC) images [Malin and Edgett, 2001] revealed that they are currently active. Sullivan *et al.* [2001] published the first detailed study of slope streaks and developed a kinematic model for dry dust avalanches consistent with observed characteristics of slope streaks. Schorghofer *et al.* [2002] correlated streak regions with surface properties including low thermal inertia, topographic roughness, and peak temperature, and suggested that transient water ice in trace amounts may play a role in triggering such avalanches. Ferris *et al.* [2002] suggested that more voluminous aqueous processes are involved in the formation of some streaks, but this hypothesis is difficult to reconcile with theoretical considerations of water stability [e.g., Ingersoll, 1970; Farmer and Doms, 1979].

[3] In this study we choose to avoid questions of slope streak triggering and formation mechanisms, but elaborate on their rates of formation and fading. The observed albedo contrast is likely due to an event that removes a (usually brighter) dusty material, exposing a (usually darker) subsurface [Sullivan *et al.*, 2001]. The varying states of fading seen in streaks are thought to result from the subsequent redeposition of dust over time. Figure 1 shows the occurrence of

new streaks at a site that has been imaged three times by MOC between 1999 and 2002, illustrating the ongoing streak formation process. The formation of these streaks is a ubiquitous process in the low-thermal inertia regions and offers insight into the Martian dust cycle.

### 2. Image Survey

[4] A survey of 29,326 MOC narrow angle images was conducted, including all images in the latitude range  $-30^\circ$  to  $60^\circ$  (Mars Global Surveyor mission phases AB1 to E12). Of the images examined, we found 1,386 to unambiguously contain slope streaks (Figure 2a). For each image containing slope streaks a set of parameters was compiled, including estimates of the numbers of dark and bright streaks in the image with associated uncertainties, azimuthal directions of dark and bright streaks, and the width of the widest streak in the image.

[5] At least 50,000 dark slope streaks and 900 bright slope streaks have been imaged in subphases AB1-E12 (Sep 1997–Jan 2002). In the low-latitude low-thermal inertia regions, one in five MOC narrow-angle images contains slope streaks, so streaks are “typical” for the dust-covered low-latitude regions. Using the number of imaged streaks, the known area of MOC images, and the fraction of MOC images with and without streaks, we estimate the areal density of streaks in MOC images to be  $\sim 0.07 \text{ km}^{-2}$  in the low-thermal inertia regions. We expect target selection biases, such as imaging slopes more frequently than flat areas, would result in an artificially increased streak density in images. If we

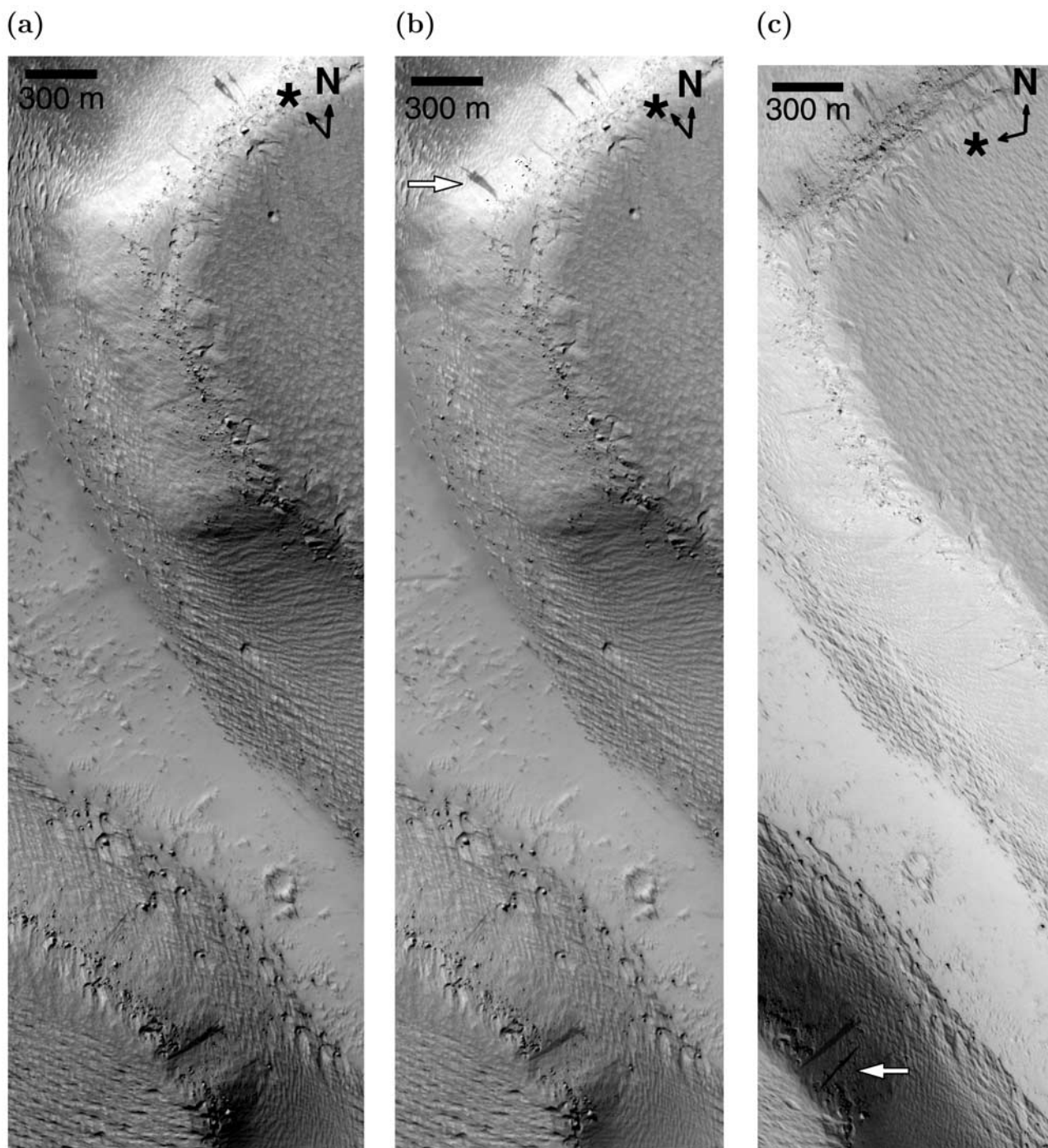


**Figure 1.** A triplet of overlap images taken on (a) 1999-03-18 (FHA-01030), (b) 2001-01-06 (M23-00388), and (c) 2002-01-03 (E12-00277). North azimuth and solar azimuth are shown in the upper right corner. Two new streaks (thick arrows) have formed at this site southwest of Daedalia Planum.

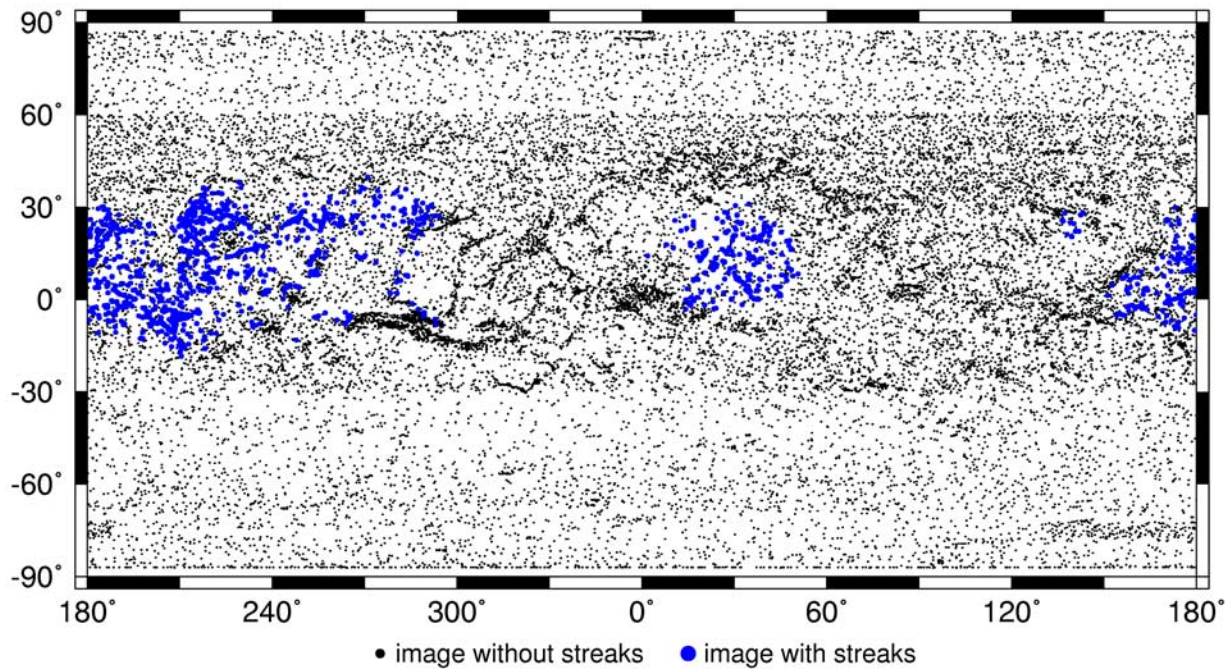
assume the average areal density is only half that in MOC images, then the roughly  $2.3 \times 10^7$  km<sup>2</sup> covered by low-thermal inertia material contain  $\sim 800,000$  streaks (on the basis of a crude extrapolation).

[6] The set of 1,386 streak images was automatically searched for overlap pairs using the image corner coordinates. This procedure identified 181 overlapping image pairs, containing  $\sim 2,500$  streaks and  $\sim 126$  new streaks.

The time difference between image pairs ranges from 7 days (E05-01337/E05-02070) to 2.2 Mars years (AB1-03104/E11-03665). The status of the image survey is summarized in Table 1, which also illustrates the rapid increase in available overlap images.

[7] Figure 2b shows the geographic distribution of the overlap images. For each pair, we recorded a count of the number of new streaks and the number of

(a)



(b)

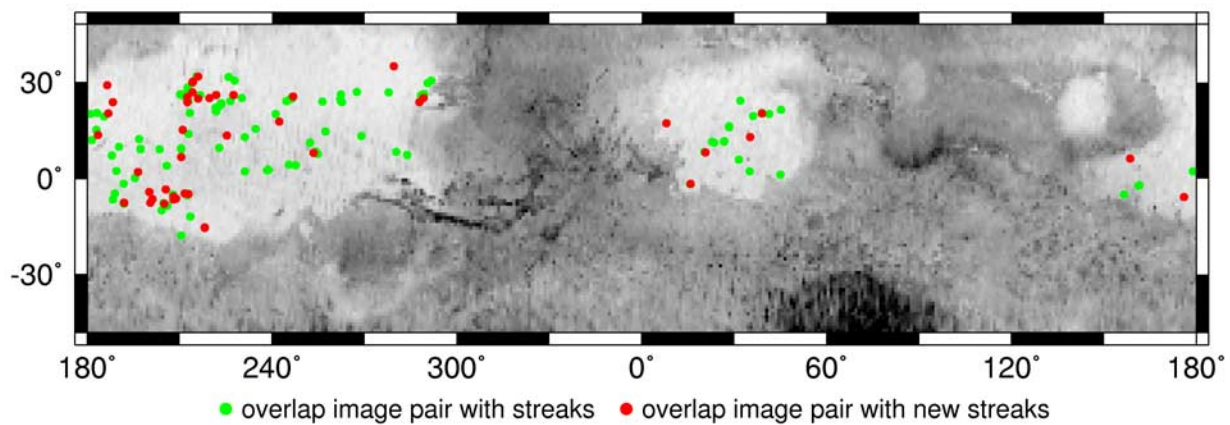


**Figure 2.** The MOC image sample used in the slope streak survey. (a) Geographic distribution of all surveyed images (small black dots) and of images containing streak (large blue dots). (b) Geographic distribution of overlap image pairs. Green dots indicate overlap image pairs with streaks, but without new streaks. Red dots show pairs with new streaks. The background gray scale is thermal inertia.

streaks in the overlap region that are visible in both images. While the feature counts are often only approximate, the presence of new streaks is unambiguous. Of the 181 image pairs, 173 allowed meaningful streak counts.

### 3. Formation Rates

[8] New streaks occur almost exclusively in areas that have preexisting streaks. Streaks remain visible in repeat

images and serve as a useful reference in discerning new streaks from observational effects. New streaks frequently have a stronger albedo contrast than streaks in the surrounding area, providing circumstantial evidence for their gradual fading.

[9] The large number of overlap image pairs enables an accurate determination of the rate of streak formation. Among the pairs where reliable streak counts are possible, about one quarter have new streaks, but this ratio grows with the time separation between images.

**Table 1.** Current Status of Our MOC Slope Streak Survey Compared to the Status of One Year Earlier<sup>a</sup>

Mission Subphases	AB-M23	AB-E12
Surveyed MOC N/A images	~23,000	~30,000
Slope streak images	~900	~1,400
Overlap pairs	44	181
Pairs with new streaks	6	48

<sup>a</sup>Overlap images provide rapidly growing amount of information about current occurrences.

[10] A formation rate  $q$  can be defined as the number of new streaks per year relative to the number of streaks in the overlap area:

$$q = \frac{\Delta n}{n\Delta t}, \quad (1)$$

where  $\Delta n$  is the number of new streaks,  $n$  the number of streaks in the overlap region (including the new streaks), and  $\Delta t$  the time interval between the two images. The number of streaks  $n$  serves as a proxy for the “propensity” of the area for streak formation, and by using it to normalize  $q$  we gain the benefit of having an area-independent measurement. The rate  $q$  is then a characteristic of the population in the sense that in steady-state, its normalization accounts for variations in factors such as slope or dust abundance.

[11] To make optimal use of the collected data, we derive robust formulae for a set of image pairs in Appendix A. Here, we will make use of the normalized probability distribution of formation rates  $P_{\chi}(q)$  (derived from equations (A2) and (A10)), the most likely rate  $\hat{q}$  which explains the observations (equations (A3) and (A11)), and the associated standard deviation  $\sigma$  (equation (A8)).

### 3.1. MOC/MOC Overlaps

[12] The probability distribution functions (PDF) derived from progressively larger subsets of MOC image pairs is shown in Figure 3, with the number of image pairs in each set indicated. The sets were broken according to the time of the later image in intervals of 6 months. (The tentative rate of 5% quoted by *Schorghofer et al.* [2002] was based on AB-M23.) The set covering the longest time interval (AB-E12) contains the largest number of image pairs, and exhibits the narrowest PDF. For this set, the most likely formation rate, assuming slow formation (equations (A3) and (A8)), is  $\hat{q} = 6.6\% \pm 0.6\%$  per streak per Martian year. The estimate is modified only slightly to  $\hat{q} = 6.8\%$  using the general formula (equation (A11)). For this relatively large set, averaging the formation rate (equation (1)) for each pair gives  $\bar{q} = 7.0\%$ . The last estimate is flawed because it weighs pairs of low statistical significance equally with pairs of high statistical significance. For subsets with fewer pairs, this inaccuracy becomes more significant.

[13] It is tempting to try to extract secular changes in the formation rate from these curves, as for example, the 41 image pairs (from AB-M23) suggest that the rate appropriate for that period is smaller by almost 2%. However, since the PDF from these time periods overlap substantially, and since observational biases change as mission phases progress, it is difficult to demonstrate a statistically significant trend.

[14] Regional variations in the formation rate can be investigated by considering only pairs occurring in restricted locales. Figure 4 shows, in map form, the variations in  $\hat{q}$

using a window of radius 900 km to filter the data. Since for a given local estimate, only a subset of the data is used, the associated errors are larger. In order to avoid plotting values where the errors are large, a value is shown only if  $\sigma < 3\%$ . The map shows that the formation rate exhibits great geographic variability, with values  $>12\%$  in western Tharsis and values of  $<5\%$ , for example in Arabia Terra. Slope streaks correlate with surface properties such as root-mean-square slope roughness and thermal inertia [*Sullivan et al.*, 2001; *Schorghofer et al.*, 2002]. Since formation rates are defined relative to the number of existing streaks, the geographic heterogeneity should not reflect variations in the local “propensity” for slope streak formation. Instead, locally higher formation rates indicate either that streaks fade (disappear) faster than average or that streak formation has accelerated.

[15] Bright streaks are less frequent than their dark counterparts by a factor of roughly 50. We have identified  $\sim 126$  new dark streaks, but have found no convincing example yet of new bright streaks. Currently, there may simply not be enough overlap images to capture a bright streak formation event.

### 3.2. Duration and Timing

[16] Figure 5 shows the time intervals for the surveyed image pairs. Streaks do not form uniformly, even at sites crowded with existing streaks. Among the pairs separated by more than one Mars year and with more than 10 streaks in the overlap, about half (10 of 22) show new streaks. In Figure 1 formation at one active site does not coincide with formation at a nearby site. We also find that the timing of streak formation cannot be explained by hypothesizing global-scale events (see Figure 5). Hence their formation appears to be of sporadic and local nature.

[17] The formation of a slope streak is expected to be a sudden and short event. The shortest time interval between image pairs with new streaks is 0.16 Mars years, or

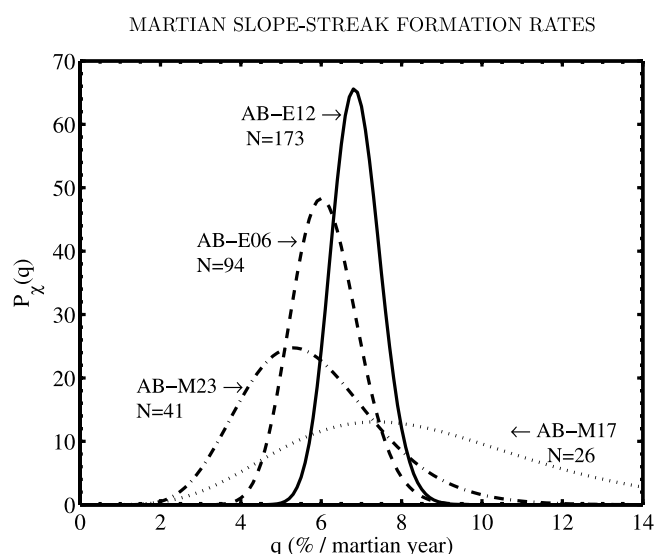


**Figure 3.** Normalized probability distribution function  $P_{\chi}(q)$  derived from MOC/MOC overlap pairs collected in various mission phases. The number of image pairs that contribute to each curve is also indicated.

## MARTIAN SLOPE-STREAK FORMATION RATES

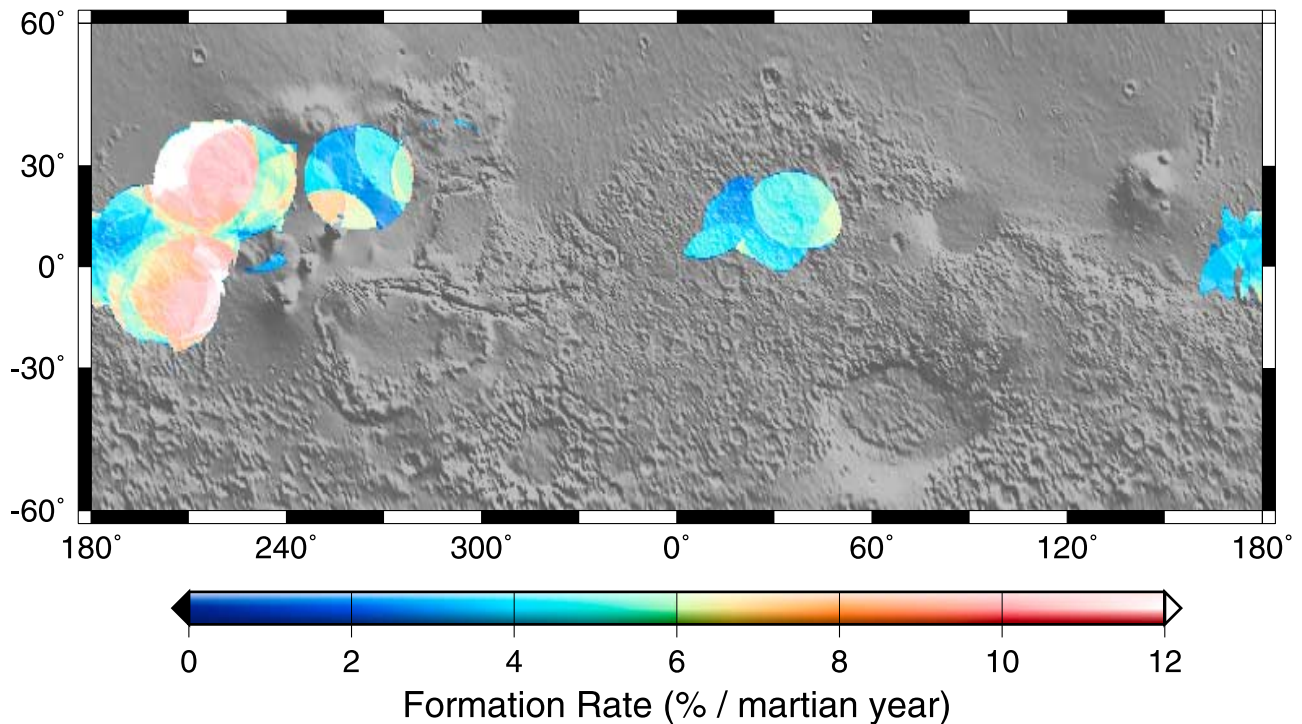


**Figure 4.** Regional variations of the slope streak formation rate. Rates are only plotted where there are at least 5 pairs and the statistical error of the local rate is less than  $\pm 3\%$ /Martian year.

109 days (M00-02492 and M03-06377, containing approximately seven streaks, one of which is new).

[18] An additional statistical constraint on the duration of an event is possible. If streaks grow over a time period  $\delta$ , then there is a finite chance that one is forming while the earlier image of the pair is taken. The probability of observing such an event is  $\Delta n\delta/\Delta t$ , for  $\delta/\Delta t \ll 1$ . We have found no conclusive evidence of growing streaks in the survey. However, it is possible that a new streak would obscure an older one. In such cases, growth of the obscured streak cannot be ruled out. An estimate of the growth rate, which depends on how many such growth events have been missed, can be obtained. For simplicity, we use the mean image time separation of  $\overline{\Delta t} = 0.7$  Mars years for all pairs. For example, if no growth events were missed then  $\delta \lesssim 8$  days at a  $2\sigma$  level. For the same confidence level and assuming one missed growth event, we obtain  $\delta \lesssim 13$  days, while if 5 were missed, then  $\delta \lesssim 29$  days. These bounds on  $\delta$  are approximate, and are presumably still much longer than the actual duration of the events.

### 3.3. Viking/MOC Overlaps

[19] A comparison with data collected 24 years ago by the Viking spacecraft allows extending the analysis to longer time-spans. The process of identifying and comparing Viking images with narrow angle MOC images is hampered by differences in resolution, instrument response, viewing geometry, and coordinate references. Nonetheless, we have found two sets of Viking-MOC pairs in which individual slope streaks can be matched. Both are located in the Olympus Mons aureole deposits. The first includes

Viking images f441b09, f441b08, and f441b02 each of which overlaps in part with MOC image E05-01067. This pair exhibits a total of 21 streaks in the overlap region, where 7 of them can be unambiguously identified as new (Figure 6). The second set consists of Viking images f441b04 and f441b05 overlapping with MOC M02-03210. These images have one streak in common, but no new ones.

[20] A crude estimate of  $\hat{q}$  going back  $\sim 12$  Mars years is possible from these comparisons. The estimated formation rate based on these two pairs alone is, from equation (A11),  $\hat{q} \sim 3\%$ . In this case  $q\Delta t$  is not small, hence the formulae in Appendix A2 are necessary. The PDFs derived from the 173 MOC only pairs and from the two Viking/MOC sites are shown in Figure 7. The tails of the PDFs overlap only slightly, and the most likely values for  $q$  are distinguishable. Analysis of MOC pairs in this region reveals an even higher than average formation rate. This suggests that slope streak formation may have accelerated. It is more rapid in the last 2 Mars years than in the last 12 Mars years. Since it is based on only two Viking-MOC pairs, this result should not be viewed as robust. Nonetheless, it is noteworthy that in the two available examples, fewer streaks than expected are observed to have formed. It is conceivable that some streaks were missed in the lower resolution Viking images. If two such ambiguous cases were counted as newly formed, the formation rate would only increase to  $\sim 4\%$ .

## 4. Fading

[21] The high formation rate of slope streaks raises the question of whether they are also observed to fade rapidly.

## MARTIAN SLOPE-STREAK FORMATION RATES

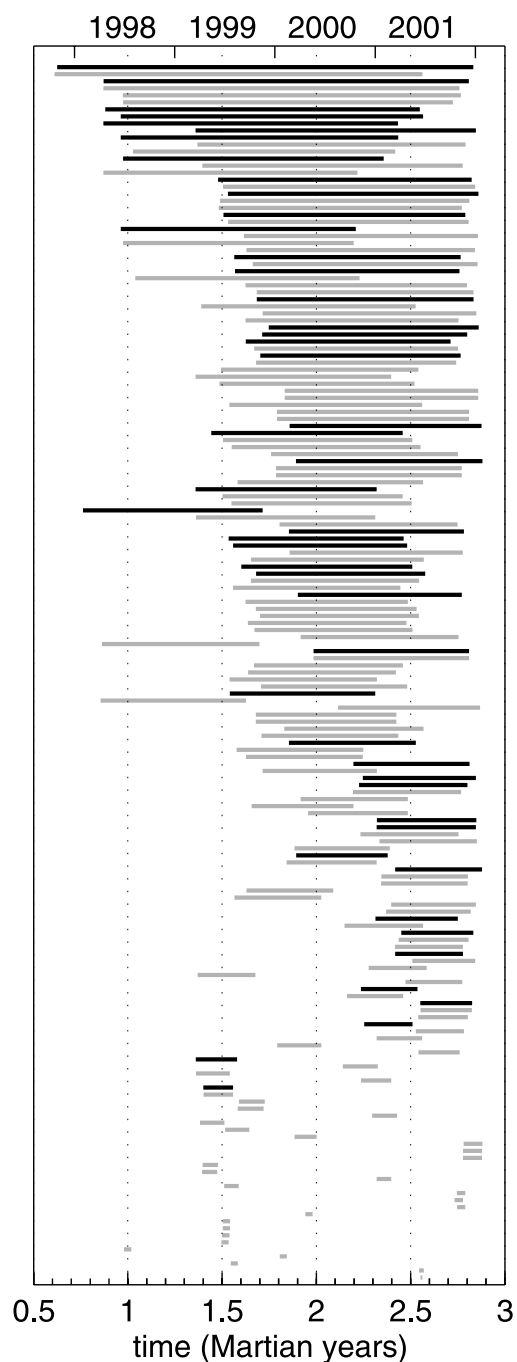


**Figure 5.** Time intervals of all 173 overlap pairs on which this study is based. Black bars indicate image pairs with new streaks and gray bars indicate pairs without new streaks. Pairs are sorted according to their time separation  $\Delta t$ . Time = 0 corresponds to the Martian vernal equinox on Aug 26, 1996.

Dust settling is expected to lead to a gradual fading of streaks. The inverse formation rate is  $1/\dot{q} \sim 15$  Martian years or  $\sim 28$  years, so observed streaks are expected to be young features. A steady state of the streak population, where the number of streaks remains roughly constant with

time, requires the formation rate to balance the fading rate. If this were the case, their albedo contrast should fade, on average,  $\sim 7\%$  a Mars year until they become invisible to MOC.

[22] More surprising than the new streaks seen since the Viking images is the fact that the old streaks are still visible (Figure 6). None seems to have disappeared and there are no apparent changes in shape or albedo. At a minimum, these streaks survived for 24 years, with no apparent modification.

[23] Terrestrial experiments [Wells *et al.*, 1984] suggest that a  $10 \text{ g/m}^2$  layer of  $1\text{--}5\mu\text{m}$  sized dust particles causes significant albedo variations. If streaks were in steady state, a fading time of  $\sim 28$  years would thus correspond to a deposition rate of  $\sim 0.4 \text{ g/m}^2/\text{yr}$  in the low-thermal inertia regions. Pollack *et al.* [1979] estimated global dust sedimentation rates of  $20 \text{ g/m}^2/\text{yr}$ , with a large fraction concentrated at the North Pole in association with  $\text{CO}_2$  condensation. The predicted spatial concentration may account for some of this apparent discrepancy. Another measurement was derived from dust accumulation upon the solar panels at the Mars Pathfinder landing site, estimated to be  $0.28\%/ \text{day}$  [Landis and Jenkins, 2000], that is,  $\sim 10 \text{ g/m}^2/\text{yr}$ . This rate was seen to decrease later in the mission, suggesting this too may overestimate the actual global annual average. In either case, streaks seen in Viking images, and still observed in MOC images (Figure 6) exhibit little change in albedo and suggest (even) smaller net deposition rates.

[24] The survival (and, in fact, unchanged morphology of) streaks from Viking to MOC observations make it unlikely that formation and fading rates are currently in balance. It appears that annual to decadal scale variations exist in one or both of these rates, and that currently fading does not keep up with the rapid formation. These variations may be gradual, or may be in the form of stochastic “bursts” of streak activity and/or fading, as might be possible after major dust storms. However, several major dust storms have been seen to envelop the planet completely since Viking images were acquired, and intermittent burial would fail to explain the low formation rate at the site photographed by Viking. Alternatively, there may be strong spatial variations in the fading rate. Deposition may be exceptionally low at the particular site of the Viking/MOC overlap images.

## 5. Conclusions

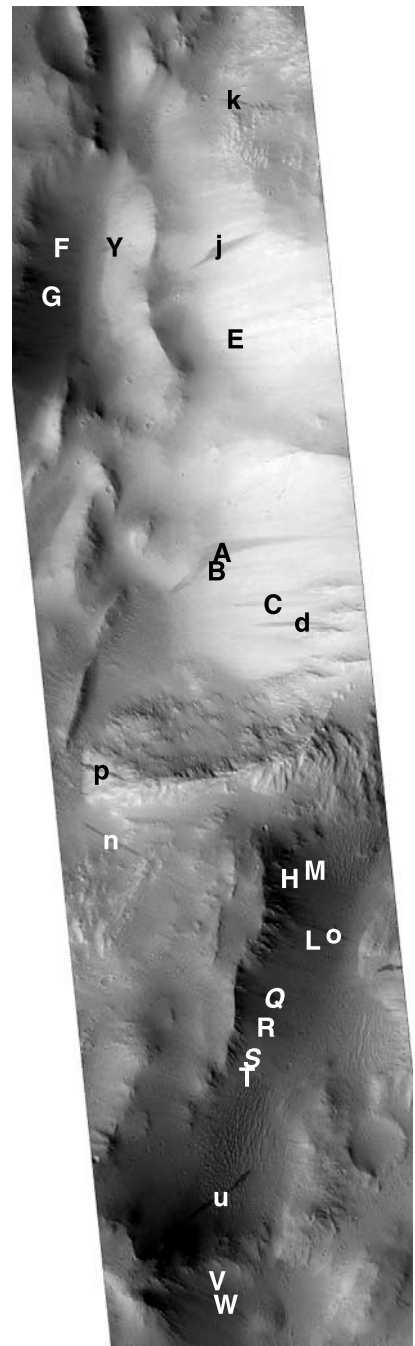
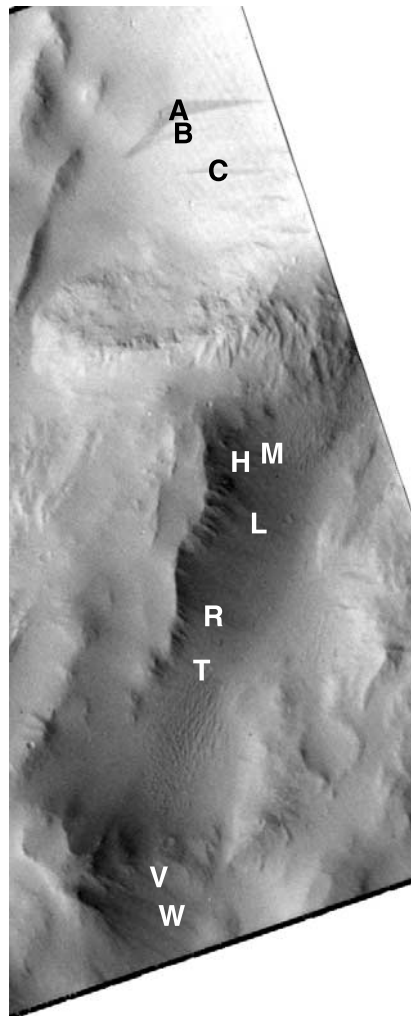
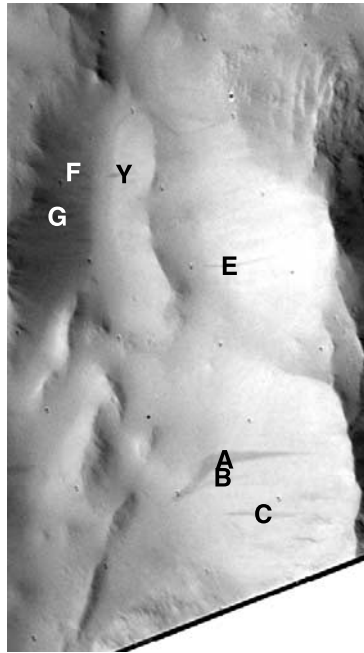
[25] New occurrences of slope streaks indicate these features are forming at a high rate of  $\sim 7\%$  per existing streak, per Martian year. Large spatial and/or temporal variations in the formation rate are seen. A steady-state condition of balance between formation and fading would imply a relatively low net deposition rate of  $\sim 0.4 \text{ g/m}^2/\text{yr}$ . The persistence of streaks over 24 years from Viking Orbiter to MOC observations suggests an even lower rate of fading and hence of dust deposition. Either gradual or stochastic variations (as would be associated with dust storms) in the dust deposition may be needed to explain the observations of changes in the formation rate, and its current imbalance with the fading rate.

MARTIAN SLOPE-STREAK FORMATION RATES

(b) 1977-11-02

(c) 1977-11-02

(d) 2001-06-11



(a)

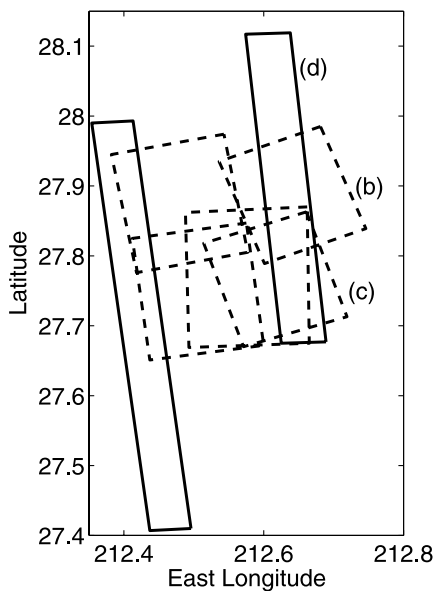


**Figure 6.** (a) Footprint map based on approximate corner coordinates of 5 Viking Orbiter images and 2 MOC images. (b, c) Viking images f441b09 and f441b08, and (d) MOC image E05-01067. Uppercase letters (A, B, C, E, F, G, H, L, M, R, T, V, W, Y) indicate preexisting streaks found in one or both of the Viking images (b, c), and lowercase letters (d, j, k, n, o, p, u) indicate new streaks in the MOC frame (d). Streaks labeled *Q* and *S* are ambiguous. Additional color stretching was necessary to assess streak matches. All streaks in f441b02 overlap are in the union of b08 and b09. North is up in all images.

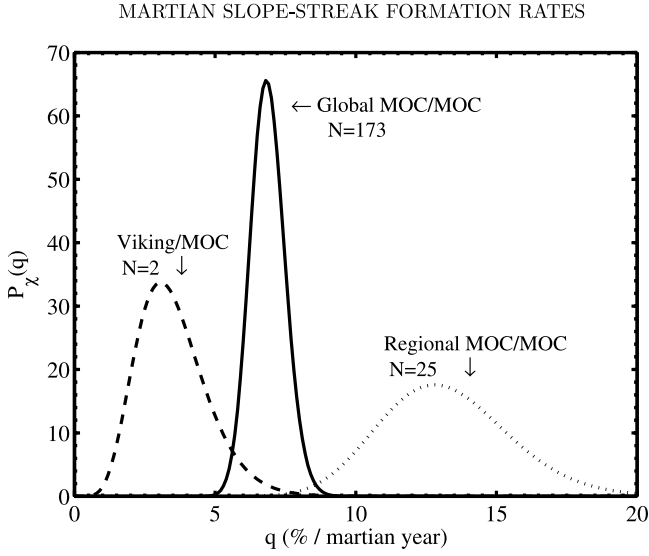


**Figure 7.** Normalized PDF (see Figure 3) derived from the MOC/MOC overlap pairs globally (solid line), MOC/MOC pairs near the Olympus Mons aureole (dotted line) and Viking/MOC pairs in that region (dashed line). The formation rate in Viking/MOC overlaps appears to be smaller than in the more recent MOC/MOC overlaps.

[26] The high relative formation rate, together with a high global abundance (estimated to be  $\sim 800,000$ ), extrapolate to an absolute formation rate of  $\sim 50,000$  per Mars year (on average  $\sim 70$  per day!). In this sense, slope streaks may be the most dynamic geologic feature observed on the surface of Mars.

[27] Due to the continuing coverage by MOC, improved constraints will be possible in the future. In addition, multiple overlap images in short time intervals could constrain the timing of streak formation. Reimaging of more of the Viking streaks would lead to a better understanding of their decadal behavior.

## Appendix A: Statistical Formulae

[28] Optimal estimates of the formation rate can be derived for data collected from multiple image pairs. It is not appropriate simply to average the expression for the formation rate for each pair  $q = \Delta n / (n \Delta t)$  because the denominator may be small due to statistical variations. Statistical (Bayesian) techniques are employed below to derive maximum likelihood estimates of the desired parameters [Papoulis, 1991].

### A1. Infrequent Formation Approximation

[29] The probability of a streak forming over a small time interval  $dt$  is  $q n dt$ , where  $n$  is the eventual number of streaks in the overlap region. The total time interval  $\Delta t$  spanned by an image pair can be divided into discrete infinitesimal intervals  $dt$ . The probability for an event to happen at a particular time is

$$\underbrace{(1 - qndt) \dots (1 - qndt)}_{\text{nothing happens}} \underbrace{qndt}_{\text{new streak}} \underbrace{(1 - qndt) \dots (1 - qndt)}_{\text{nothing happens}}$$

Given a formation rate  $q$ , the resulting probability for  $\Delta n$  events at any time is

$$\begin{aligned} p(\Delta t, n, \Delta n | q) &= \lim_{dt \rightarrow 0} \binom{\Delta t / dt}{\Delta n} (1 - qndt)^{\frac{\Delta t}{dt} - \Delta n} (qndt)^{\Delta n} \\ &= \frac{1}{\Delta n!} e^{-qn\Delta t} (qn\Delta t)^{\Delta n}. \end{aligned} \quad (\text{A1})$$

The total probability of the set of observations  $\chi = \{n_i, \Delta n_i, \delta t_i\}$ , is

$$\begin{aligned} P(\chi | q) &= \prod_i p(\Delta t_i, n_i, \Delta n_i | q) \\ &= \prod_i \frac{1}{\Delta n_i!} e^{-qn_i \Delta t_i} (qn_i \Delta t_i)^{\Delta n_i}. \end{aligned} \quad (\text{A2})$$

The index  $i = 1, \dots, N$  runs over all image pairs.

[30] The most likely formation rate  $q = \hat{q}$  is the value that maximizes  $P(\chi | q)$ , that is, where  $dP/dq = 0$ . This can be solved to yield the rate  $\hat{q}$  that best explains the observations:

$$\hat{q} = \frac{\sum_i \Delta n_i}{\sum_i n_i \Delta t_i}. \quad (\text{A3})$$

The sum is over all image pairs.

[31] To invert  $P(\chi | q)$  in order to obtain the probability distribution function of  $q$  given the set of observations  $\chi$ , we make use of the identity

$$P(q | \chi) P(\chi) = P(\chi | q) P(q), \quad (\text{A4})$$

and assume a priori that lacking any knowledge  $q$  is uniformly distributed ( $P(q)$  is constant). Hence

$$P(q | \chi) = \frac{P(\chi | q) P(q)}{\int_0^\infty P(\chi | q) P(q) dq} = \frac{P(\chi | q)}{P_o}, \quad (\text{A5})$$

where the zeroth moment is

$$\begin{aligned} P_o &= \int_0^\infty P(\chi | q) dq \\ &= \left( \prod_i \frac{(n_i \Delta t_i)^{\Delta n_i}}{\Delta n_i!} \right) \left( \sum_j n_j \Delta t_j \right)^{-1 - \sum_k \Delta n_k} \sum_k \Delta n_k!. \end{aligned}$$

As a shorthand, we refer to the PDF in equation (A5) as  $P_\chi(q) = P(q | \chi)$ , which is simply  $P(\chi | q)$  normalized. Similarly, the expectation values of  $q$  and  $q^2$  are

$$\langle q \rangle = \int_0^\infty q P(q | \chi) dq = \frac{1 + \sum_i \Delta n_i}{\sum_i n_i \Delta t_i} \quad (\text{A6})$$

and

$$\langle q^2 \rangle = \int_0^\infty q^2 P(q | \chi) dq = \frac{(1 + \sum_i \Delta n_i)(2 + \sum_i \Delta n_i)}{(\sum_i n_i \Delta t_i)^2}. \quad (\text{A7})$$

For the standard deviation  $\sigma$ , we obtain

$$\sigma = \left\langle (q - \langle q \rangle)^2 \right\rangle^{1/2} = \frac{\langle q \rangle}{\sqrt{1 + \sum_i \Delta n_i}}, \quad (\text{A8})$$

which is an estimate of the statistical uncertainty.

## A2. Rapid Formation

[32] A more general (but less explicit) expression may be derived if the assumption of slow formation rate is relaxed. In this case the probability of any particular sequence of events is

$$\begin{aligned} & [1 - q(n - \Delta n + 1)dt] \dots \underbrace{q(n - \Delta n + 1)dt}_{\text{1st streak}} \dots \\ & \dots [1 - q(n - 1)dt] \dots \underbrace{qndt}_{\text{last streak}} [1 - qndt] \dots [1 - qndt]. \end{aligned}$$

Let  $t_1 < t_2 < \dots < t_{\Delta n}$  denote the times when streaks form. After taking the limit as  $dt \rightarrow 0$ ,

$$p(\Delta t, n, \Delta n; t_1, \dots, t_{\Delta n} | q) = q^{\Delta n} e^{qn\Delta t} e^q \sum_{j=1}^{\Delta n} t_j n! / (n - \Delta n)!$$

Since actual formation times are unknown, it is again necessary to sum over all possibilities:

$$\begin{aligned} p(\Delta t, n, \Delta n | q) &= \int_0^{\Delta t} dt_1 \int_{t_1}^{\Delta t} dt_2 \dots \int_{t_{\Delta n-1}}^{\Delta t} dt_{\Delta n} \\ &\quad \times q^{\Delta n} e^{qn\Delta t} e^q \sum_{j=1}^{\Delta n} t_j n! / (n - \Delta n)! \\ &= \binom{n}{\Delta n} e^{-qn\Delta t} (e^{q\Delta t} - 1)^{\Delta n}. \end{aligned} \quad (\text{A9})$$

The boundaries of all integrals can be changed to 0 and  $\Delta t$ , by introducing a prefactor of  $1/(\Delta n)!$  [e.g., *Peskin and Schroeder*, 1995]. The probability of a given set of observations  $\chi$  is modified from equation (A2) to

$$P(\chi | q) = \prod_i \binom{n_i}{\Delta n_i} e^{-qn_i \Delta t_i} (e^{q\Delta t_i} - 1)^{\Delta n_i}. \quad (\text{A10})$$

The value  $\hat{q}$  that maximizes  $P(\chi | q)$  is now given by the transcendental equation,

$$0 = \sum_i \frac{\Delta n_i \Delta t_i}{1 - e^{-\hat{q} \Delta t_i}} - n_i \Delta t_i, \quad (\text{A11})$$

which can be solved numerically. The expressions in equations (A10) and (A11) reduce to those in equations (A2) and (A3) in the limit where  $q\Delta t \ll 1$  and  $\Delta n \ll n$ .

## A3. Event Duration

[33] Given  $\Delta n$  events over a time interval  $\Delta t$ , each event of duration  $\delta$ , the probability of observing  $m$  events in progress is

$$P(m | \delta) = \binom{\Delta n}{m} \left(1 - \frac{\delta}{\Delta t}\right)^{\Delta n - m} \left(\frac{\delta}{\Delta t}\right)^m. \quad (\text{A12})$$

The probability distribution of  $\delta$ , given  $m$  events, is

$$P(\delta | m) = P(m | \delta) \frac{P(\delta)}{P(m)} = \frac{\Delta n + 1}{\Delta t} P(m | \delta). \quad (\text{A13})$$

where  $P(\delta)$  was assumed to be uniform in the interval between 0 and  $\Delta t$ . The expectation value is

$$\langle \delta \rangle = \int \delta P(\delta | m) d\delta = \frac{m + 1}{\Delta n + 2} \Delta t. \quad (\text{A14})$$

Similarly, the standard deviation  $\sigma_\delta$  is

$$\sigma_\delta = \sqrt{\frac{n - m + 1}{(m + 1)(n + 3)}} \langle \delta \rangle. \quad (\text{A15})$$

[34] Note that even if no growth events are observed ( $m = 0$ ), the expected value of  $\delta$  is non-zero. Furthermore, for large  $\Delta n$  and  $m$ , (A14) reduces to  $\langle \delta \rangle = (m/\Delta n)\Delta t$  as might be expected.

[35] **Acknowledgments.** We wish to thank Glenn Bennett and Lori Fenton for help with ISIS processing of Viking images, Mark Richardson for discussions concerning the Martian dust cycle, Re'em Sari for a conversation on Bayesian statistics, and Robert Sullivan and Vic Baker for helpful reviews. This study was supported by NASA's Mars Data Analysis Program, grant NAG 5-13232.

## References

- Farmer, C. B., and P. E. Doms, Global and seasonal variation of water vapor on Mars and the implications for permafrost, *J. Geophys. Res.*, *84*, 2881–2888, 1979.
- Ferguson, H. M., and B. K. Lucchitta, Dark streaks on talus slopes, Mars, in *Planetary Geology and Geophysics Program Report*, NASA Tech. Memo., 86246, 188–190, 1984.
- Ferris, J. C., J. M. Dohm, V. R. Baker, and T. Maddock, Dark slope streaks on Mars: Are aqueous processes involved?, *Geophys. Res. Lett.*, *29*(10), 1490, doi:10.1029/2002GL014936, 2002.
- Ingersoll, A. P., Mars: Occurrence of liquid water, *Science*, *168*, 972–973, 1970.
- Landis, G. A., and P. P. Jenkins, Measurement of the settling rate of atmospheric dust on Mars by the MAE instrument on Mars Pathfinder, *J. Geophys. Res.*, *105*, 1855–1858, 2000.
- Malin, M. C., and K. S. Edgett, Mars Global Surveyor Mars Orbiter Camera: Interplanetary cruise through primary mission, *J. Geophys. Res.*, *106*, 23,429–23,570, 2001.
- Morris, E., Aureole deposits of the Martian volcano Olympus Mons, *J. Geophys. Res.*, *87*, 1164–1178, 1982.
- Papoulis, A., *Probability, Random Variables, and Stochastic Processes*, 3rd ed., McGraw-Hill, New York, 1991.
- Peskin, M. E., and D. V. Schroeder, *Introduction to Quantum Field Theory*, Westview, Boulder, Colo., 1995.
- Pollack, J. B., D. S. Colburn, F. M. Flasar, R. Kahn, C. E. Carlston, and D. Pidek, Properties and effects of dust particles suspended in the Martian atmosphere, *J. Geophys. Res.*, *84*, 2929–2945, 1979.
- Schorghofer, N., O. Aharonson, and S. Khattiwala, Slope streaks on Mars: Correlations with surface properties and the potential role of water, *Geophys. Res. Lett.*, *29*(23), 2126, doi:10.1029/2002GL015889, 2002.
- Sullivan, R., P. Thomas, J. Veverka, M. Malin, and K. S. Edgett, Mass movement slope streaks imaged by the Mars Orbiter Camera, *J. Geophys. Res.*, *106*, 23,607–23,633, 2001.
- Wells, E. N., J. Veverka, and P. Thomas, Mars—Experimental study of albedo changes caused by dust fallout, *Icarus*, *58*, 331–338, 1984.